JPE 19-2-25

https://doi.org/10.6113/JPE.2019.19.2.602
ISSN(Print): 1598-2092 / ISSN(Online): 2093-4718

Double-Loop Coil Design for Wireless Power Transfer to Embedded Sensors on Spindles

Suiyu Chen*, Yongmin Yang†, and Yanting Luo*

†,*Science and Technology on Integrated Logistics Support Laboratory,
National University of Defense Technology, Changsha, China

Abstract

The major drawbacks of magnetic resonant coupled wireless power transfer (WPT) to the embedded sensors on spindles are transmission instability and low efficiency of the transmission. This paper proposes a novel double-loop coil design for wirelessly charging embedded sensors. Theoretical and finite-element analyses show that the proposed coil has good transmission performance. In addition, the power transmission capability of the double-loop coil can be improved by reducing the radius difference and width difference of the transmitter and receiver. It has been demonstrated by analysis and practical experiments that a magnetic resonant coupled WPT system using the double-loop coil can provide a stable and efficient power transmission to embedded sensors.

Key words: Embedded sensors, Magnetic resonant coupled, Spindle, WPT

I. INTRODUCTION

Almost all modern electromechanical systems are driven by spindles. Thus, it is necessary to monitor the running status of spindles to ensure the reliability and security of these systems [1]. Sensors are often embedded on spindles since they can be installed close enough to the faulty sections to increase accuracy. However, the power supply to these embedded sensors remains a major obstacle [2]. There are several conventional power supply methods including battery charging, wired charging and slipring charging. However, battery charging needs frequent replacements due to its limited capacity, which is rather inconvenient. In addition, the spindle is winded if wired charging is applied. Slipring charging is also unsuitable since slipring wears easily with the rotation of spindles [3]-[5].

Non-radiative wireless power transfer (WPT) technology provides a potential solution to this problem. This technology is divided into two kinds: inductive coupling and magnetic resonant coupling. Both of these are based on the electromagnetic coupling mechanism. However, the power transmission efficiency of inductive coupled WPT systems is greatly affected by the angular and axial misalignments between the transmitter and receiver. In addition, its transmission distance is limited to a few centimeters [6]-[10]. When compared to inductive coupling WPT systems, magnetic resonant coupled WPT systems can transfer power efficiently over a longer distance (tens of centimeters), and its efficiency is less affected by low coupling due to misalignment. Moreover, environmental factors such as humidity, temperature and non-ferromagnetic objects have little impact on transmission [7], [11]-[13]. Powering embedded sensors on a spindle using this technology has become a hot issue.

A basic magnetic resonant coupled WPT system consists of a primary coil (transmitter) and a secondary coil (receiver), two resonant capacitors, a high-frequency AC power source and a load. By adjusting the capacitors, the coils can be tuned to match the operating frequency. Thus, power can be transmitted efficiently from the transmitter to the receiver [14], [15]. However, when applied to embedded sensors, this system cannot maintain a high transmission efficiency or a stable power output due to variations of the transmission distance, obstructions of the spindle, and magnetic flux leakage [16], [17].

For solving this problem, a design consisting of two transmitters and three receivers (2T3R) was proposed in [18]. As shown in Fig. 1(a), the three receivers are symmetrically distributed around the spindle and two transmitters are fixed at

Manuscript received Mar. 7, 2018; accepted Dec. 13, 2018
Recommended for publication by Associate Editor Byungtaek Kim.
†Corresponding Author: 291639140@qq.com
Tel: +86-13308491488, Fax: +86-0731-87005507, National University of Defense Technology
*Science and Technology on Integrated Logistics Support Laboratory, National University of Defense Technology, China

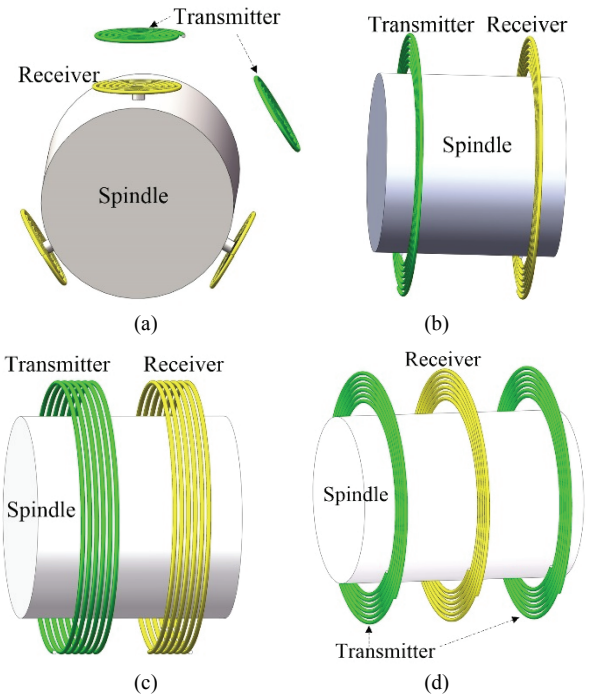

Fig. 1. Configurations of existing coil designs. (a) 2T3R. (b) Coaxial spiral. (c) Coaxial helical. (d) Sandwiched.

60° intervals. The efficiency degradation caused by one receiver rotating away from the transmitters can be compensated by the next receiver coming into range. However, the efficiency fluctuation range is still large, the average efficiency is low and an increasing number of coils makes it more difficult to tune the system. Due to these disadvantages, it is not applicable and will not be discussed further in this paper.

Typical coaxial spiral coils and helical coils have been used for this problem [1], [19]-[21], as shown in Fig. 1(b) and Fig. 1(c). It should be noted that both of these two types of coils can be concentric, which occurs when the transmission distances decrease to zero and the radiuses of the transmitter and receiver are unequal to avoid interference. These two configurations are also simple to manufacture, install and tune. They usually have different applications depending on the installation spaces. Coaxial spiral coils are often installed on faces perpendicular to the axis, such as bearing faces and flywheel faces. Meanwhile, helical coils are usually placed on smooth spindle surfaces. Although these two types of coils are simple enough in practical applications, their power transmission performances are poorer than the following sandwiched and double-loop coil designs.

As shown in Fig. 1(d), a sandwiched coil design has proposed, which consists of two separate stationary transmitters and a single receiver sandwiched between them [22]. Together, the two transmitters produced stronger and more directive magnetic fields than a single spiral coil. Thus, this design provides enhanced magnetic coupling. However, it requires more complex tuning units, which interfere with the operation of spindles due to their large weight and size.

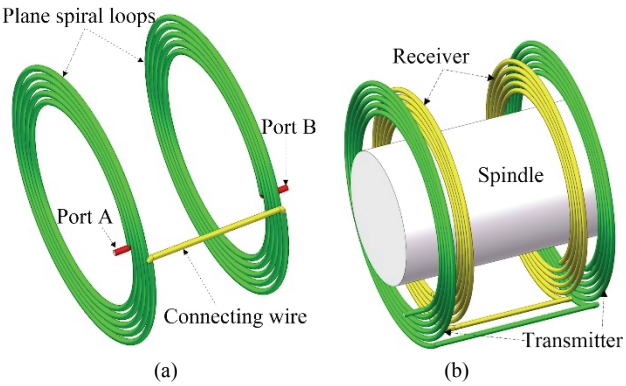

Fig. 2. Configuration of double-loop coil design. (a) Single coil. (b) Two coils placed coaxially.

The main difficulties in terms of wirelessly charging the embedded sensors on spindles lie in power transfer instability, weak coupling and tuning complexity. To solve these problems, a novel double-loop coil design is proposed in this paper, as shown in Fig. 2(a). It consists of two coaxial plane spiral loops and a connecting wire integrating them. Fig. 2(b) shows that the two double-loop coils, which are used as a transmitter and a receiver, are coaxially and symmetrically placed. When compared to the existing coil designs, this design has the advantages of tuning simplicity and enhanced power transmission performance. The main difference lies in the fact that the double-loop coil integrates the two plane spiral loops so that it can greatly enhance the magnetic coupling by using tuning units as that are as simple as coaxial spiral and coaxial helical designs.

The rest of this paper is organized as follows. In Section II, the efficiency expression of a magnetic resonant coupled WPT system is derived. In addition, the mechanism of the double-loop coil is illustrated and its characteristics are investigated by a theoretical analysis. Then in Section III, the magnetic field distribution of a single double-loop coil, the variations of the power transfer capacity with the coil radius and coil width, and the performance when compared with existing coil designs are all simulated via finite-element analysis (FEA). Practical experiments are conducted in Section IV to verify the characteristics of the proposed design. This is followed by some conclusions in Section V.

II. Theoretical Analysis

A. Analysis of a Magnetic Resonant Coupled WPT System

Fig. 3 shows an equivalent circuit model of a magnetic resonant coupled WPT system. R_S, L_S, C_S and I_S are the primary-side resistance, inductance, capacitance and current, respectively. Meanwhile, R_D, L_D, C_D and I_D belong to the second side. U_S, M and R_0 are the AC power source voltage, mutual inductance and load, respectively.

By Kirchhoff's Law, it is possible to obtain:

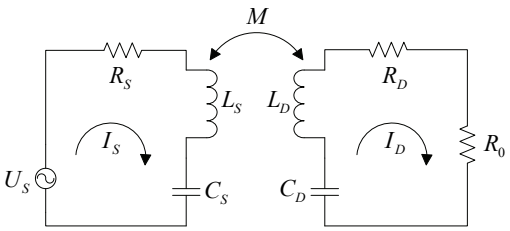

Fig. 3. Equivalent circuit model of a magnetic resonant coupled WPT system.

$$\begin{bmatrix} R_S + j\omega L_S + \dfrac{1}{j\omega C_S} & -j\omega M \\ -j\omega M & R_D + R_0 + j\omega L_D + \dfrac{1}{j\omega C_D} \end{bmatrix} \begin{bmatrix} I_S \\ I_D \end{bmatrix} = \begin{bmatrix} U_S \\ 0 \end{bmatrix} \quad (1)$$

where ω is the operating frequency, i.e., the AC power source frequency. Thus, the power transmission efficiency can be derived as:

$$\eta = \left|\frac{I_D^2 R_0}{U_S I_S}\right| = \frac{1}{R_D + R_0 + j\left(\omega L_D - \dfrac{1}{\omega C_D}\right)} \times \frac{\omega^2 M^2 R_0}{\left[R_S + j\left(\omega L_S - \dfrac{1}{\omega C_S}\right)\right]\left[R_D + R_0 + j\left(\omega L_D - \dfrac{1}{\omega C_D}\right)\right] + \omega^2 M^2} \quad (2)$$

When $\omega = 1/\sqrt{L_S C_S} = 1/\sqrt{L_D C_D}$, i.e., the system is tuned, the efficiency can be written as:

$$\eta = \frac{\omega^2 M^2 R_0}{\left[R_S (R_D + R_0) + \omega^2 M^2\right](R_D + R_0)} \quad (3)$$

From Equ. (3), the efficiency increases with the mutual inductance. In addition, the mutual inductance increases with the flux linkage in the transmitter and receiver. When the receiver rotates away from the transmitter, the flux linkage decreases sharply due to misalignment and obstruction of the metallic spindle, which can lead to an efficiency drop. The proposed double-loop coil keeps its mutual inductance high and stable. As a result, power is transmitted efficiently and stably.

B. Analysis of Double-Loop Coil

In a double-loop coil setup, as shown in Fig. 4, the transmitter is stationary and the receiver is attached to the spindle, and both of them are coaxially placed with the spindle. The non-metallic layer provides space for the magnetic path. When current flows through the coil, the current directions in the two loops of the same coil are opposite. Between the loops, the magnetic fields generated by the two loops radially reinforce and axially cancel out each other. When not between the loops, they cancel out each other both radially and axially.

The proposed coil integrates two plane spiral loops and has a magnetic field coupling that is significantly stronger than a single pair of conventional single-loop coils. In addition, the magnetic field generated by the transmitter passing through either of the cylinders and bottom surface of the receiver can induce a current. According to Lenz's Law, the two currents corresponding to the cylinder surface and the bottom surface flow in the same direction. Thus, the current flowing through the receiver is enhanced. Moreover, since the two loops are integrated by a connecting wire into a single coil, the WPT system is easier to tune than multi-coil designs, such as 2T3R and sandwiched coils.

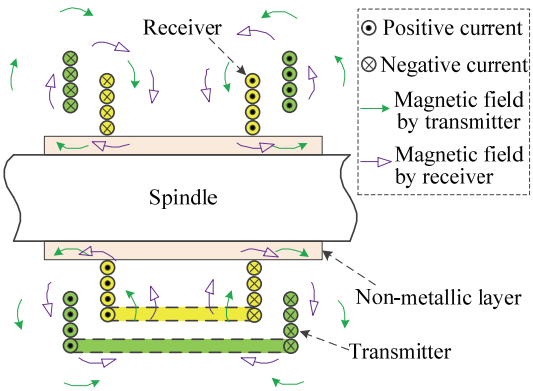

Fig. 4. Currents and magnetic fields of two coaxial double-loop coils.

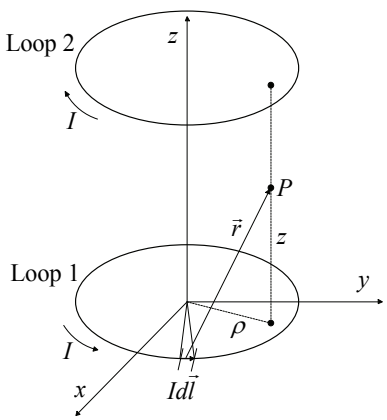

Fig. 5. Model of a single double-loop coil.

Fig. 5 shows a model of a single double-loop coil. Since the connecting wire has little effect on the whole magnetic field, only the two spiral loops are considered for the sake of simplicity, and they are represented with two coaxial circles. The currents flowing in the two loops are equal and opposite in direction. In this figure, I is the current, w is the distance between the loops, i.e., the coil width, R is the coil radius, $Id\vec{l}$ is an arbitrary current element in Loop 1, P is an arbitrary point in space, and $\vec{r}$ is the vector from $Id\vec{l}$ to point P. In addition, $(R, \beta, 0)$ and (ρ, α, z) are the cylindrical coordinates of $Id\vec{l}$ and point P, respectively.

According to Biot-Savart Law, the flux density of the magnetic field produced by $Id\vec{l}$ is given by:

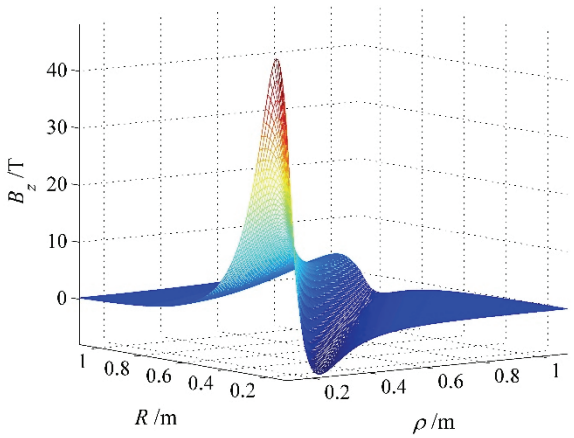

(a)

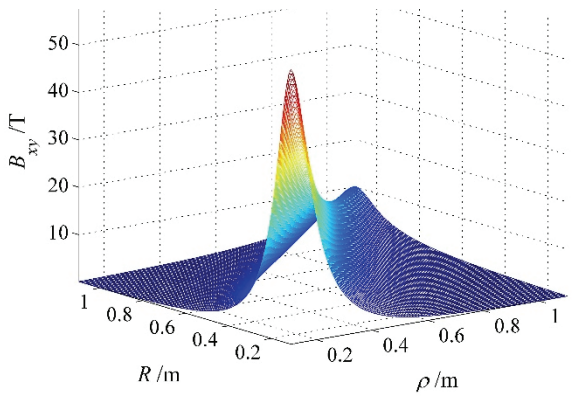

(b)

Fig. 6. Variation of B_z and B_{xy} with ρ and R. (a) B_z . (b) B_{xy} .

$$d\vec{B} = \frac{\mu_0 Id\vec{l} \times \vec{r}}{4\pi r^3} \tag{4}$$

where μ_0 is permeability of vacuum. The flux density produced by the current of Loop 1 is:

$$\vec{B}_1 = \frac{\mu_0 I}{4\pi}\int_0^{2\pi} \frac{Rz\left(\cos\beta\vec{e}_x + \sin\beta\vec{e}_y\right) + \left(R^2 - R\rho\cos(\beta-\alpha)\right)\vec{e}_z}{\left(\sqrt{\rho^2+R^2+z^2-2\rho R\cos(\beta-\alpha)}\right)^3} d\beta \tag{5}$$

where $\vec{e}_x$, $\vec{e}_y$ and $\vec{e}_z$ are the unit vectors in the x, y and z directions, respectively. The flux density produced by the current of Loop 2 can be easily obtained through the same procedure as:

$$\vec{B}_2 = \frac{\mu_0 I}{4\pi}\int_0^{2\pi} \left[\frac{R(w-z)\left(\cos\beta\vec{e}_x + \sin\beta\vec{e}_y\right)}{\left(\sqrt{\rho^2+R^2+(w-z)^2-2\rho R\cos(\beta-\alpha)}\right)^3} - \frac{\left(R^2 - R\rho\cos(\beta-\alpha)\right)\vec{e}_z}{\left(\sqrt{\rho^2+R^2+(w-z)^2-2\rho R\cos(\beta-\alpha)}\right)^3} \right] d\beta \tag{6}$$

Thus, the total flux density $\vec{B}$ can be obtained by adding $\vec{B}_1$ and $\vec{B}_2$ together, or by:

$$\vec{B} = \vec{B}_{xy} + \vec{B}_z \tag{7}$$

where $\vec{B}_{xy}$ and $\vec{B}_z$ represent the xy-plane and the z components of $\vec{B}$. Let $\beta = \theta + \alpha$. Thus, $\vec{B}_{xy}$ and $\vec{B}_z$ can be derived from Eqns. (5)-(7) as follows:

$$\vec{B}_{xy} = B_{xy}\left(\cos\alpha\vec{e}_x + \sin\alpha\vec{e}_y\right) \tag{8}$$

$$\vec{B}_z = B_z\vec{e}_z = \frac{\mu_0 IR\vec{e}_z}{2\pi}\int_0^{\pi} \left[\frac{-\rho\cos\theta + R}{\left(\sqrt{(\rho-R)^2+z^2+2\rho R(1-\cos\theta)}\right)^3} - \frac{-\rho\cos\theta + R}{\left(\sqrt{(\rho-R)^2+(w-z)^2+2\rho R(1-\cos\theta)}\right)^3} \right] d\theta \tag{9}$$

where B_{xy} is given by:

$$B_{xy} = \frac{\mu_0 IR}{2\pi}\int_0^{\pi} \left[\frac{z\cos\theta}{\left(\sqrt{(\rho-R)^2+z^2+2\rho R(1-\cos\theta)}\right)^3} + \frac{(w-z)\cos\theta}{\left(\sqrt{(\rho-R)^2+(w-z)^2+2\rho R(1-\cos\theta)}\right)^3} \right] d\theta \tag{10}$$

From Equ. (8) and Equ. (10), the direction of $\vec{B}_{xy}$ is radial. In Equ. (9) and Equ. (10), the first items in the square brackets correspond to the magnetic field produced by Loop 1, and the second items correspond to Loop 2. The interaction of the two magnetic fields generated by the two loops can be analyzed through these corresponding items. Thus, when $z \in (0, w)$, i.e., point P is between the loops, the two magnetic fields reinforce each other radially (in the xy direction), and cancel out each other out axially (in the z direction). In particular, when $z = w/2$, $B_z = 0$ and then $\vec{B} = \vec{B}_{xy}$. Thus, when $z = w/2$, the direction of $\vec{B}$ becomes radial. This characteristic improves the magnetic flux through the cylinder surface of the double-loop receiver. When $z \notin (0, w)$, the two fields cancel each other out both radially and axially. From Eqns. (7)-(10), the magnitude of $\vec{B}$ is independent of α . This means that when point P rotates around the z axis, the magnitude of the magnetic flux at point P remains unchanged. This characteristic keeps the flux linkage in the receiver unchanged when the receiver rotates along with the spindle, which stabilizes the power transmission.

Fig. 6 illustrates the variations of B_z and B_{xy} with ρ and R via

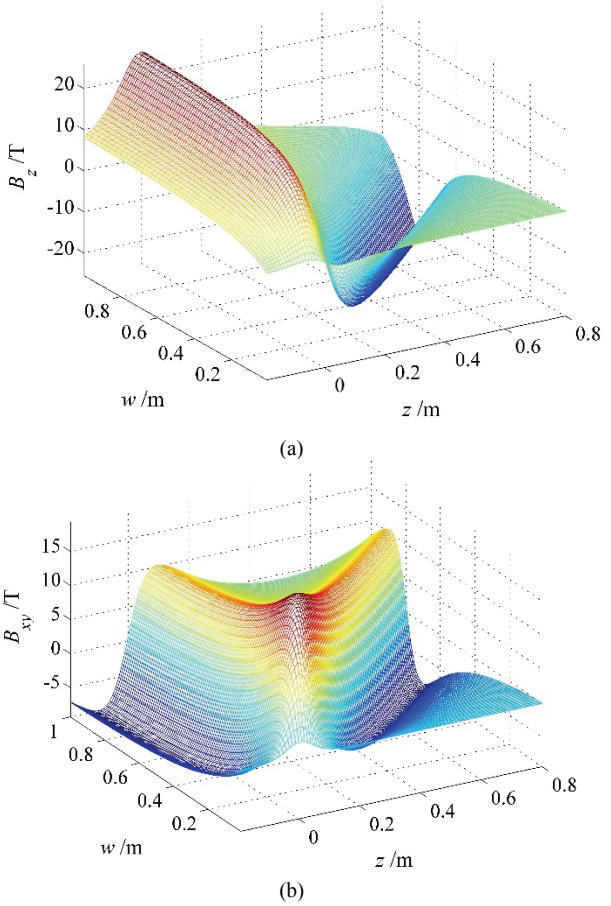

Fig. 7. Variations of B_z and B_{xy} with z and w: (a) B_z ; (b) B_{xy} .

the numerical calculation method according to Equ. (9) and Equ. (10). From Fig. 6(a), when R is identical, B_z increases with ρ and is maximized when ρ is nearly equal to R. Then it drops sharply to below zero, which means that the direction of $\vec{B}_z$ is reversed. From Fig. 6(b), when R is identical, B_{xy} increases with ρ and is maximized when ρ=R. Then it decreases. It is indicated that $|\vec{B}|$ can be maximized when ρ approaches R. Thus, by reducing the radius difference between the transmitter and the receiver, the flux linkage between them can be increased. Note that the connecting wire can be extended to avoid the interference of the transmitter and receiver. In Fig. 6(b), when both ρ and R increase and their difference remains unchanged, B_z and B_{xy} decrease. This is because the current elements become farther away from point P when ρ and R increases together, which lowers the flux density produced by each current element in point P.

Fig. 7 shows the variations of B_z and B_{xy} with z and w. It has been proved that when $z = w/2$, $B_z = 0$. In Fig. 7(a), when $z < w/2$, $B_z > 0$; and when $z > w/2$, $B_z < 0$. This means that the direction of $\vec{B}_z$ on one side of the middle plane is opposite that of the other side. In addition, when $z = 0$ or $z = w$, $|B_z|$ is maximized. In Fig. 7(b), when z is nearly equal to 0 or w, B_{xy} is maximized. Moreover, when $z < 0$ or $z > w$, $B_{xy} < 0$. This indicates that the direction of $\vec{B}_{xy}$ between the loops is opposite to that outside the loops. It can be concluded that $|\vec{B}|$ can be maximized when z approaches 0 or w. Thus, the flux linkage between the transmitter and the receiver can be increased by reducing their width difference. It can also be seen that when $|z - w/2|$ is identical, both B_z and B_{xy} remain unchanged. This corresponds to the symmetry of the proposed double-loop coil.

TABLE I
SIMULATION PARAMETERS FOR A SINGLE DOUBLE-LOOP COIL

Parameters	Values
Coil radius	50mm
Wire radius	1mm
Number of turns	5
Coil width	50mm
Direct current	1A
Coil material	Copper

III. FINITE-ELEMENT ANALYSIS

A. Magnetic Field Simulation of a Single Coil

To identify the magnetic properties of the double-loop coil, a 3D-FEA model of a single coil is built. For the sake of simplicity, cross sections of the loops are replaced by rectangles. Direct current is applied to the coil. The simulation parameters for this model are given in Table I. The results are shown in Fig. 8.

Fig. 8(a) shows the direction and intensity of the magnetic field generated by a single double-loop coil. It can be seen that the direction of the field produced by Loop 1 is opposite that of Loop 2, which indicates that the two fields radially reinforce and axially cancel each other out between loops. In addition, the fields are mainly concentrated near the two loops. As shown in Fig. 8(b), the flux density is identical on the same horizontal plane, which indicates that the flux linkage in receiver remains stable when it rotates with the spindle. This characteristic ensures the stability of the power transmission. In addition, it also shows that the flux density gets larger as it approaches the two loops.

For further verification of Eqns. (7)-(10), the flux density data of different paths in the simulation model shown in Fig. 8 is extracted. The point (0,30,10) is chosen as the reference point of the analysis, and two paths are set crossing this point. The paths parallel to the y-axis and the z-axis are denoted as path A and path B, respectively. Through data processing, the components of the flux density on these paths can be acquired.

Fig. 9 shows variations of the flux density components with the distances from the z-axis, ρ (path A) and z-coordinate (path B). It can be seen from Fig. 9(a) that B_z changes its sign and that

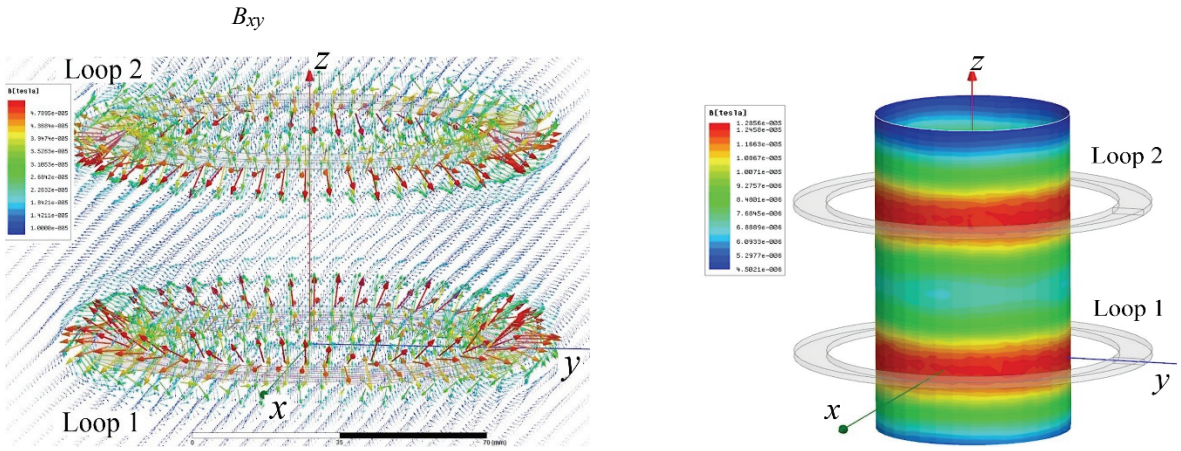

(a) (b)

Fig. 8. Magnetic field simulation of a single coil. (a) Direction and intensity. (b) Flux density on a cylindrical surface with a bottom radius of 30 mm.

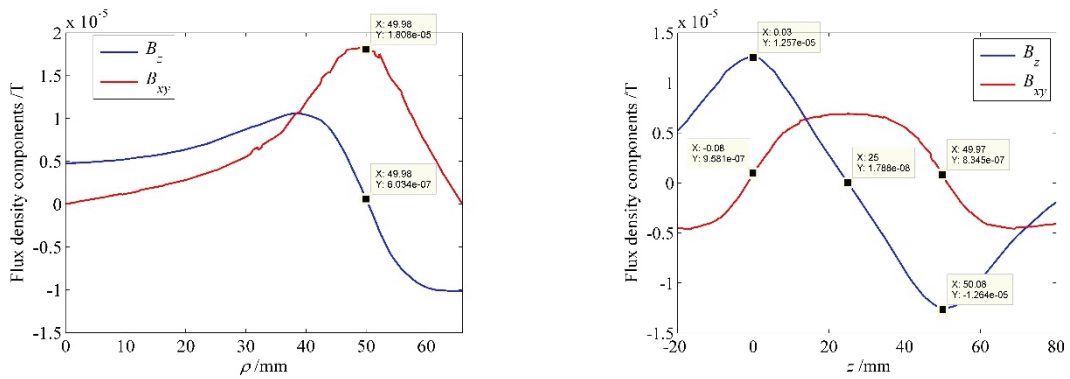

(a) (b)

Fig. 9. Variation of the flux density components on two paths. (a) Path A. (b) Path B.

is maximized as ρ approaches 50 mm. In addition, the radius of the coil R, which indicates that any point with a distance from the z-axis close to R can be a critical point for the z-direction of the magnetic field. Furthermore, the field directions at these points are parallel to the xy-plane. From Fig. 9(b), the magnitude of B_z is maximized as z approaches 0mm or 50 mm, and it reduces to zero as z approaches 25 mm, which demonstrates that B_z on the middle plane of the coil is roughly equal to zero. In addition, B_{xy} changes its sign when z approaches 0 mm or 50 mm.

All in all, the variation curves in Fig. 9 coincide with Fig. 6 and Fig. 7, which verifies the characteristics derived from the analytical equations for the flux density.

B. Power Transmission Simulation of Two Coils

A 2D-FEA model consisting of two double-loop coils, which are coaxially and symmetrically placed, is built according to Table II. The alternating current applied to the transmitter is given by $I=I_A\sin(2\pi ft)$, which induces an alternating voltage in the receiver. Since the load value is unknown, the amplitude of the induced voltage E_A can be used as an indicator of the power transmission capacity of the coil. To study the effects of the coil radius and coil width on the transmission capacity, the radius and width of the receiver are varied and E_A can be measured. The results are shown in Fig. 10.

TABLE II
SIMULATION PARAMETERS FOR TWO DOUBLE-LOOP COILS

Parameters	Values
Radius of transmitter, R_1	50mm
Radius of receiver, R_2	10mm - 80mm
Width of transmitter, w_1	50mm
Width of receiver, w_2	10mm - 40mm
Number of turns, N_1=N_2	5
Wire radius	1mm
I_A	1A
f	1MHz
Coil material	Copper

From Fig. 10(a), E_A is maximized when R_2=R_1=50mm. Moreover, it decreases with the difference between R_1 and R_2.

This phenomenon can be explained with the variation of B_z with ρ as shown in Fig. 9(a). When $R_2>R_1$, the direction of B_z when $\rho<R_1$ is opposite the direction when $R_1<\rho<R_2$, which causes a counteraction of the magnetic flux. This characteristic

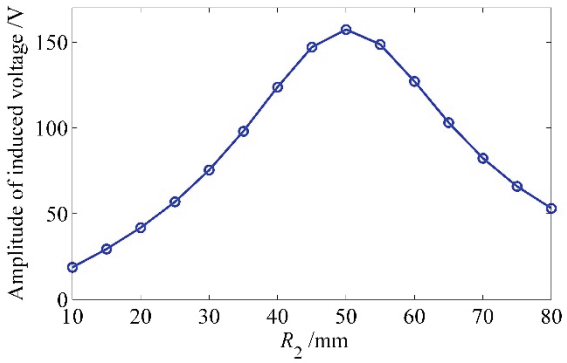

(a)

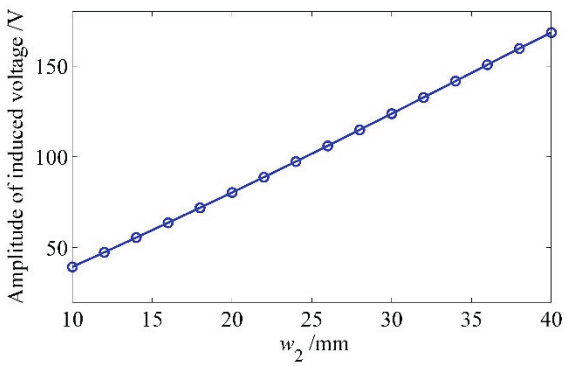

(b)

Fig. 10. Variation of the amplitude of the induced voltage. (a) With R_2 (w_2=30mm). (b) With w_2 (R_2=40mm).

TABLE III
SIMULATION PARAMETERS FOR ALL OF THE COILS

Parameters	Values
Radiuses of transmitters	50mm
Radiuses of receivers	40mm
Number of turns, N_1=N_2	5
Wire radius	1mm
Coil material	Copper
Spindle radius	30mm
Spindle material	Iron

indicates that in order to enhance the power transmission capability, R_2 should be set as close to R_1 as possible, instead of enlarging either R_1 or R_2 without regard to each other. It can be seen from Fig. 10(b) that E_A almost linearly increases with w_2. Since w_2 is usually less than w_1, enlarging w_2 is a feasible method for improving the power transmission capability.

C. Performance Comparison of Different Coil Designs

To compare the performance of the proposed double-loop coil with existing coil designs, 2D-FEA models of different coils with transmission distances of D=0mm (The coils are concentric and coaxial) and D=10mm are built according to Table III. Accordingly, the double-loop coil width was set to w_1=100mm, w_2=80mm and 100mm. The transmission distance of the double-loop coil is equal to half of its width difference.

TABLE IV
SIMULATION RESULTS FOR DIFFERENT COILS (D = 0 mm)

Coil type	E_A (V) No spindle	E_A (V) With Spindle	M (μH)
Coaxial spiral	143.59	75.08	0.9155
Coaxial helical	132.88	65.31	0.8479
Sandwiched	285.75	149.12	1.8219
Double-loop	252.08	147.07	1.6070

TABLE V
SIMULATION RESULTS FOR DIFFERENT COILS (D = 10 mm)

Coil type	E_A (V) No spindle	E_A (V) With Spindle	M (μH)
Coaxial spiral	115.69	51.20	0.7365
Coaxial helical	115.78	50.82	0.7378
Sandwiched	231.25	100.59	1.4732
Double-loop	189.78	95.16	1.2100

The currents applied to the transmitters are the same as those in Table II. The simulation results are shown in Table IV and Table V.

From Table IV and Table V, the coaxial spiral coils and helical coils have similar values for E_A and M, which are less than the E_A and M of the proposed double-loop coil design. This indicates that the coaxial spiral coil and helical coil have similar power transmission performance, which is poorer than that of the double-loop coil. However, the values of E_A and M of the double-loop coil are slightly less than the E_A and M of the sandwiched coil. This can be counteracted by the easier tuning characteristic of the double-loop coil. Thus, with consideration of the power transmission performance and tuning complexity, the double-loop coil design has advantages over existing coil designs.

IV. EXPERIMENTAL VERIFICATION

As shown in Fig. 11(a), the proposed double-loop coil is made from a continuous piece of Litz wire supported by two holders. In addition, it consists of two loops and a connecting wire. The turn number of each loop is N=5. The radius and strand number of the Litz wire are 1.5mm and 400, respectively. Using Litz wire can effectively reduce the skin effect and proximity effect of the coil at high frequencies. This lowers the loss of the resistance caused by these two effects. As shown in Fig. 11(b), the transmitter and receiver are separated and coaxially placed. The connecting wire transmitter can be extended to avoid interference with the receiver.

As shown in Fig. 12, a magnetic resonant coupled WPT system using double-loop coils is built to verify the conclusions drawn by the theoretical and finite-element analyses in Section II and Section III. The receiver is coaxially placed with and attached to a metallic spindle. The transmitter is coaxial and separated from them. The power amplifier receives a signal

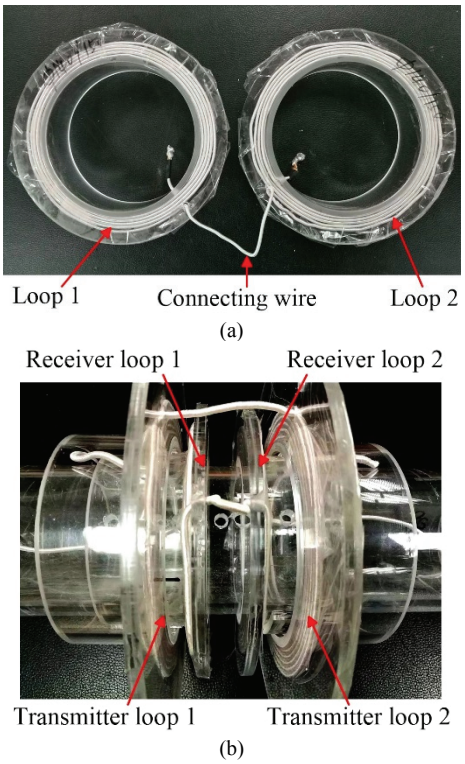

Fig. 11. Pictures of double-loop coils. (a) Single coil. (b) Transmitter and receiver.

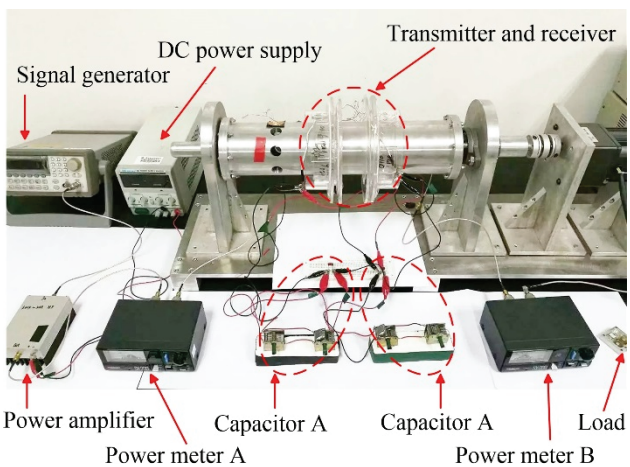

Fig. 12. Picture of a magnetic resonant coupled WPT system using double loop coils.

from the signal generator, and power from a DC power supply, which provides a high-frequency alternating current for the transmitter. The system can be tuned by adjusting the two capacitors. Finally, the power output is provided for the load. Two power meters are used to measure the power input and output.

In order to experiment on the impact of the coil radius on the power transmission efficiency, the following settings are used f = 1 MHz, w_1 = 50 mm, w_2 = 30 mm. First R_2 = 60 mm is kept and R_1 is changed from 50 mm to 80 mm by 10 mm. Then R_1 = 60 mm is kept and R_2 is changed from 50 mm to 80 mm by

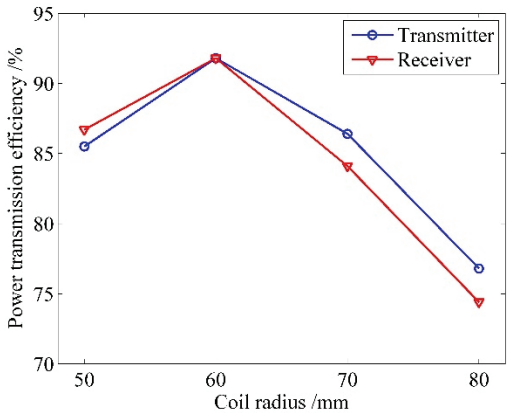

Fig. 13. Variation of the power transmission efficiency with the coil radius.

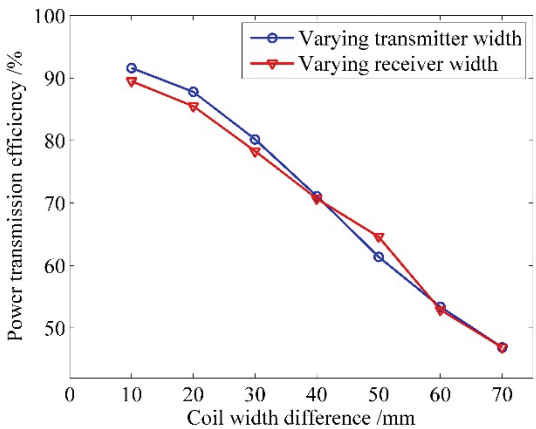

Fig. 14. Variations of power transmission efficiency with coil width differences.

10 mm. Thus, the effects caused by radius variations of both the transmitter and receiver can be observed. The system is tuned and the efficiency corresponding to different coil radiuses can be calculated by measuring the power inputs and outputs. Experimental results are shown in Fig. 13.

From Fig. 13, no matter which radius is changed, the efficiency increases with the coil radius, and is maximized when $R_1 = R_2$. Then it decreases. This demonstrates that the efficiency decreases with the coil difference $|R_1 - R_2|$.

For experimental research on the relation between coil width and efficiency, the following settings are used f = 1 MHz, R_1 = 60 mm, R_2 = 50 mm. First w_2 = 30 mm is kept and w_1 is varied from 40 mm to 100 mm by 10 mm. Then w_1 = 100 mm is kept and w_2 is changed from 30 mm to 90 mm by 10 mm. Efficiencies corresponding to varied coil widths are obtained. For comparison, a variation curve of the efficiency with the width difference $|w_1 - w_2|$ is drawn, which is shown in Fig. 14.

From Fig. 14, when w_1 or w_2 is varied, the efficiency decreases with $|w_1 - w_2|$. Moreover, it can be seen that when $|w_1 - w_2|$ is identical, the efficiencies when varying w_1 are close to those when varying w_2. This shows that the width

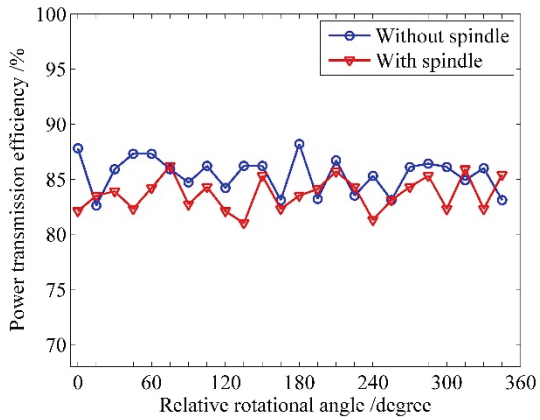

Fig. 15. Variations of power transmission efficiency with relative rotational angles.

difference, rather than w_1 or w_2, has a major impact on efficiency. The reason is that the flux linkage between the transmitter and the receiver is nearly unchanged when $|w_1 - w_2|$ remains the same, which keeps the mutual inductance nearly unchanged.

In addition to the impacts of coil radiuses and widths, the relative rotation between the transmitter and the receiver as well as the effect of the metallic spindle needs to be experimentally studied. First, the following settings are used f = 1 MHz, R_1 = 60 mm and R_2 = 50 mm. Then the relative rotational angles of the transmitter and receiver are varied from 0° to 345° by 15°. Then the efficiencies corresponding to these angles after tuning the system are obtained. To study the effect of the metallic spindle, experiments are performed with and without a metallic spindle. The results are shown in Fig. 15.

From Fig. 15, when the receiver turns to different angles, the efficiency varies a little around 85%. In addition, the efficiencies measured in the absence of a spindle are close to those in the presence of a spindle. This demonstrates that a magnetic resonant coupled WPT system using the proposed double-loop coil can provide an efficient and stable power supply to the embedded sensors on a spindle. Moreover, the system is barely affected by a metallic spindle.

V. Conclusions

This paper proposed a novel double-loop coil design for powering embedded sensors on a spindle via magnetic resonant coupled WPT technology. The proposed design has the following advantages.

(1) It avoids complex tuning units. The two loops are integrated into a single coil with the help of a connecting wire, which makes it easier to tune the system than multi-coil designs such as 2T3R and sandwiched coils.

(2) It provides efficient power transmission. It has better power transmission performance and a larger mutual inductance than existing coaxial spiral and helical coils. In addition, its tuning simplicity offsets its disadvantage over the sandwiched coil design in terms of power transmission performance.

(3) It provides a stable power supply. Since the magnetic field generated by the transmitter is axisymmetric, the coupling status between the transmitter and the receiver remains stable since the receiver rotates along with the spindle.

In addition, the power transmission efficiency decreases with the coil radius difference and the width difference. The characteristics of the proposed coil have been successfully verified through theoretical, FEA and experimental methods.

Acknowledgment

The authors greatly appreciate the support provided by the National Basic Research Program of China (Grant No. 2015 CB057404), the National Natural Science Foundation of China (Grant No. 51375485) and the Natural Science Foundation of Hunan Province (Grant No. 2017JJ2300).

References

[1] M. Rizal, J. A. Ghani, M. Z. Nuawi, and H. C. H. Che, "A wireless system and embedded sensors on spindle rotating tool for condition monitoring," *Adv. Sci. Lett.*, Vol. 20, pp. 1829-1832, Oct. 2014.

[2] M. Maier and N. Parspour, "Operation of an electrical excited synchronous machine by contactless energy transfer to the rotor," in *Proc. IPEMC*, pp. 625-630, 2016.

[3] M. Maier, M. Hagl, M. Zimmer, J. Heinrich, and N. Parspour, "Design and construction of a novel rotating contactless energy transfer system for an electrical excited synchronous machine," in *Proc. ICEM*, pp. 709-714, 2016.

[4] B. A. Potter and S. A. Shirsavar, "Design, implementation and characterization of a contactless power transfer system for rotating applications," in *Proc. ACIIE*, pp. 2168-2173, 2006.

[5] Y. T. Luo, Y. M. Yang, and Z. S. Chen, "Network analysis and impedance matching methods for wireless power transfer via coupled magnetic resonances," in *Proc. ICIDMP*, pp. 301-305, 2013.

[6] W. Zhang, J. Wjite, and C. C. Mi, "Loosely coupled transformer structure and interoperability study for EV wireless charging systems," *IEEE Trans. Power Electron.*, Vol. 30, No. 11, pp. 6356-6367, Nov. 2015.

[7] S. D. Barman, A. W. Reza, N. Kumar, M. E. Karim, and A. B. Munir, "Wireless powering by magnetic resonant coupling: Recent trends in wireless power transfer system and its applications," *Renew. Sust. Energ. Rev.*, Vol. 51, pp. 1525-1552, Nov. 2015.

[8] K. André, K. Aristeidis, M. Robert, J. D. Joannopoulos, F. Peter, and S. Marin, "Wireless power transfer via strongly coupled magnetic resonances," *Science*, Vol. 317, No. 5834, pp. 83-86, Jul. 2007.

[9] B. H. Waters, B. J. Mahoney, V. Ranganathan, and J. R. Smith, "Power delivery and leakage field control using an adaptive phased array wireless power system," *IEEE Trans.*

Power Electron., Vol. 30, No. 11, pp. 6298-6309, Nov. 2015.
[10] H. C. Bo, E. S. Lee, Y. H. Sohn, G. Jang, and C. T. Rim, "Six degrees of freedom mobile inductive power transfer by crossed dipole Tx and Rx coils," *IEEE Trans. Power Electron.*, Vol. 31, No. 4, pp. 3252-3272, Apr. 2016.
[11] T. Kan, T. D. Nguyen, J. C. Wjite, R. K. Malhan, and C. Mi, "A new integration method for an electric vehicle wireless charging system using LCC compensation topology: analysis and design," *IEEE Trans. Power Electron.*, Vol. 32, No. 2, pp. 6130-6140, Feb. 2017.
[12] J. Deng, W. Li, T. D. Nguyen, S. Li, and C. C. Mi, "Compact and efficient bipolar coupler for wireless power chargers: design and analysis," *IEEE Trans. Power Electron.*, Vol. 30, No. 11, pp. 1638-1650, Nov. 2015.
[13] S. Nakamura, M. Namiki, Y. Sugimoto, and H. Hashimoto, "Q controllable antenna as a potential means for wide-area sensing and communication in wireless charging via coupled magnetic resonances," *IEEE Trans. Power Electron.*, Vol. 32, No. 1, pp. 218-232, Jan. 2017.
[14] E. Gati, G. Kampitsis, and S. Manias, "Variable frequency controller for inductive power transfer in dynamic conditions," *IEEE Trans. Power Electron.*, Vol. 32, No. 2, pp. 1684-1696, Feb. 2017.
[15] C. C. Huang, C. L. Lin, and Y. K. Wu, "Simultaneous wireless power/data transfer for electric vehicle charging," *IEEE Trans. Ind. Electron*., Vol. 64, No. 1, pp. 682-690, Jan. 2017.
[16] R. Trevisan and A. Costanzo, "A 1-kW contactless energy transfer system based on a rotary transformer for sealing rollers," *IEEE Trans. Ind. Electron*., Vol. 61, No. 11, pp. 6337-6345, Nov. 2014.
[17] D. C. Ludois, M. J. Erickson, and J. K. Reed, "Aerodynamic fluid bearings for translational and rotating capacitors in noncontact capacitive power transfer systems," *IEEE Trans. Ind. Electron*., Vol. 50, No. 2, pp. 1025-1033, Mar. 2014.
[18] G. B. Lee, H. C. Gwak, Y. S. Kim, and W. S. Park, "Wireless power transfer system for diagnostic sensor on rotating spindle," in *Proc. IWPT*, pp.100-102, 2013.
[19] A. Abdolkhani and A. P. Hu, "Face to face through-hole contactless slipring system for rotary applications," *Int. J. Adv. Res. Elec., Electron. Instrum. Eng.*, Vol. 2, No. 9, pp. 4277-4286, Sep. 2013.
[20] A. Abdolkhani, A. P. Hu, and N.-K. C. Nair, "Modelling and parameters identification of through-Hole type wind turbine contactless sliprings," *Engineering*, Vol. 4, pp. 272-283, 2012.
[21] M. S. Carmeli, F. Castelli-Dezza, M. M. Maglio, and M. Mauri, "Design and Analysis of a high frequency wireless power feeding system for train axle telemetry," in *Proc. SPEEDAM*, pp. 527–532, 2014.
[22] A. Abdolkhani, A. P. Hu, and N.-K. C. Nair, "A double stator through-hole type contactless slipring for rotary wireless power transfer applications," *IEEE Trans. Energ. Convers.*, Vol. 29, No. 2, pp. 426-434, Jun. 2014.

Suiyu Chen was born in Zhangzhou, China, in 1992. He received his B.S. and M.S. degrees in Mechanical Engineering from the National University of Defense Technology, Changsha, China, in 2014 and 2016, respectively. He is currently working towards his Ph.D. degree in Mechanical Engineering at the National University of Defense Technology. His current research interests include magnetic resonant coupled wireless power transfer and blade tip timing measurement.

Yongmin Yang was born in Changde, China, in 1966. He received his B.S. and M.S. degrees in Automatic Control from the Nanjing University of Science and Technology, Nanjing, China, in 1987 and 1990, respectively. He received his Ph.D. degree in Information and Communication Engineering from the National University of Defense Technology, Changsha, China, in 2015. He worked with the Department of Mechanical Engineering, National University of Defense Technology, as an Assistant Professor from 1990 to 1992; and as a Lecturer from 1992 to 1998. From 1998 to 1999, he was a Visiting Scholar at the Department of Mechanical Engineering, University of California, Berkeley, CA, USA. From 1998 to 2003, he was an Associate Professor at the School of Mechatronics Engineering and Automation, National University of Defense Technology, where he has been a Professor since 2003. His current research interests include embedded diagnosis and prognostics, nonlinear system identification, the application of smart materials and structures in fault detection, integrated diagnosis and condition-based maintenance.

Yanting Luo received his B.S., M.S. and Ph.D. degrees in Mechanical Engineering from the National University of Defense Technology, Changsha, China, in 2011, 2014 and 2018, respectively. His current research interests include magnetically coupled resonant wireless power transfer and wireless/near-field communication system.